EPJ manuscript No.
(will be inserted by the editor)

Multi-year cycles observed in air temperature data and proxy series

G. Mabille[1] and S. Nicolay[2,a]

[1] Department of Physical Geography. University of Liège
[2] Department of Mathematics. University of Liège

Abstract. First, palaeoclimatic time series are analyzed under the lens of the continuous wavelet transform. Two cycles, of period 30 and 43 months respectively, are detected in millennial temperature reconstructions. These rhythms correspond to the ones detected in weather station temperature records in a previous study of the authors. It is then showed that most parts of the globe are affected by at least one of the two cycles. Their relationship with the main climatic indices is also investigated, as well as the statistical significance of the observations.

1 Introduction

New tools in signal analysis allow to extract sharper information from times series. In particular, the wavelet transform has already been applied in numerous climatic studies (see e.g. [1,2]; see also [3] for a review). Recently, unexpected periods have been observed in temperature data and climatic indices (see e.g. [4–7]). In [5], the scale spectrum – a wavelet-based tool – is used to reveal the existence of two cycles, whose periods are about 30 and 43 months respectively.

Here, we describe this approach in more details and apply it to palaeoclimatic data, namely the temperature reconstruction time series of Jones et al. [8] (these data are split into the Northern and the Southern Hemisphere) and the EPICA DOME C ice core deuterium data [9]. The scale spectrum of the ice core data ascertains the validity of the method, while the spectrum of the Jones temperature data corroborates the results concerning the 30 and 43 months period cycles obtained in [5]. Next it is shown, using the NCEP/NCAR reanalysis data and the most complete air surface temperature time series obtained from European Climate Assessment & Dataset (ECAD) and Goddard Institute for Space Studies (GISS), that every region on the globe is affected by either one of these cycles. Their relationship with the major climatic indices (namely NAO, AO and ENSO) influencing the climate is also explored. The areas mainly affected by the ENSO index display a cycle corresponding to 43 months, while the areas under the influence of the AO-NAO indices exhibit a 30 months period cycle. Finally, the statistical relevance of the observed rhythm is checked.

This study shows the remarkable stability of the periods previously observed; they are detected on the whole planet, no matter the period covered or the sample period used.

2 Data

First, we briefly describe the data used in this study.

[a] e-mail: S.Nicolay@ulg.ac.be

2.1 EPICA Dome C Ice cores deuterium data

EPICA (*European Project for Ice Coring in Antarctica*) Dome C ice core deuterium data [9, 10] gives reliable informations concerning the past climate on Earth during the last 800,000 years period. Estimating the isotopic fraction of deuterium in ice cores H_2O molecules allows to determinate the Earth's climate including the air temperature occurring during the snowfalls in the past. These data can be found at `ftp://ftp.ncdc.noaa.gov`.

The resolution of the record goes from 70 years to 5000 years (for the oldest data). Linear interpolation has been used to obtain equi-sampled data. Let us notice that such a method can not introduce any artefact in the shape of the associated scale spectrum (see subsection 3.3): if the mother wavelet has several vanishing moments, the wavelet coefficients corresponding to the linear parts are equal to zero (see subsection 3.2).

2.2 Millennial temperature reconstructions

Two thousand years long hemispheric temperature records (NH10 and SH7) are used in this study. They have been obtained by averaging 17 temperature reconstructions from proxy-data (see [8]). The data, available at `ftp://ftp.ncdc.noaa.gov`, are normalized with the 1961-90 mean temperature, and represent, in this way, the temperature anomalies during the last millennium.

2.3 CRU air temperature data

From the $5\,^\circ \times 5\,^\circ$ grid-box basis CRUTEM3 data file, we have used the monthly hemispheric anomalies during the 1950-2007 period. In this work, we have opted to choose the same period to compute all the scale spectra from the temperature data time series. The CRUTEM3 data file is available on the CRU (Climate Research Unit) website `http://www.cru.uea.ac.uk`.

2.4 Temperature time series from individual weather stations

The air surface temperatures used in this study have been collected from the European Climate Assessment & Dataset (ECAD) [11] (daily sampled) and Goddard Institute for Space Studies (GISS) [12] (monthly sampled) data sets; the Uccle (Belgium) surface air temperature data have been obtained through the IRM (`meteo.be`). Only the most complete records have been chosen for the time period corresponding to 1950–2007; older data are often missing, sparse or less reliable. These data can be found at the websites `http://eca.knmi.nl/` and `http://www.giss.nasa.gov/`.

2.5 NCEP/NCAR reanalysis data

The air surface temperatures from the NCEP/NCAR reanalysis time series [13] were selected as a gridded data set. Such a signal represents the state of the Earth's atmosphere, incorporating observations and global climate output. Let us notice that the data from the oceans must be carefully interpreted, since the number observations for such grid points is rather small.

2.6 Climatic indices

The NAO CPC index [14], which characterizes the strength of the Westerlies, is constructed from the 500 mb height anomalies over the Northern Hemisphere. The AO index [15] is estimated from the 1,000 mb height anomalies poleward of 20° N. The ENSO index (global-SST ENSO) is obtained from the sea surface temperature anomalies in the equatorial zone and takes into account the SST poleward of 20° N. The data are available on the JISAO website `http://jisao.washington.edu/data_sets/globalsstenso/`.

3 Method

The scale spectrum is a wavelet-based method that allows to detect rhythms in non-stationary signals. In this section, we first define the continuous wavelet transform and show how it can be used in the frequency domain. Finally, we introduce the scale spectrum and explain why it can be a useful tool for the study of "slowly evolving" non-stationary signals.

3.1 The continuous wavelet transform

We briefly introduce the continuous wavelet transform of a function.

Let us first give the mathematical definition (for more details, see [16–18]). A wavelet (or mother wavelet) is a function ψ belonging to $L^1(\mathbb{R}) \cap L^2(\mathbb{R})$ that satisfies the admissibility condition

$$\int \frac{|\hat{\psi}(\omega)|^2}{|\omega|} d\omega < \infty,$$

where $\hat{\psi}$ denotes the Fourier transform of ψ. For such a condition to be satisfied, the equality $\hat{\psi}(0) = 0$ has to hold (but this condition is not sufficient). In other words, the first moment of ψ vanishes, which explains the denomination "wavelet". The continuous wavelet transform (CWT) is the operator defined as follows,

$$W : L^2(\mathbb{R}) \to L^2\left(\mathbb{R} \times \mathbb{R}_*^+; dt\frac{da}{a}\right) \quad f \mapsto \int f(x)\bar{\psi}\left(\frac{x-t}{a}\right)\frac{dx}{a},$$

where $\bar{\psi}$ denotes the complex conjugate of ψ.

The CWT was first introduced in [19] and [20] for analyzing seismic data and acoustic signals. It can be regarded as a mathematical microscope (see [21]), for which position and magnification correspond to t and $1/a$ respectively, the performance of the optic being determined by the mother wavelet. This tool has been successfully put into practice on numerous theoretical and applied problems (see e.g. [22–24,17,18]).

3.2 Wavelets for frequency-based studies

One of the possible applications of the CWT is the investigation of the frequency domain of a function.

Let us show that the CWT is an effective tool for frequency-based studies. For such a study, the mother wavelet ψ has to satisfy a second condition: it has to belong to the Hardy space $H^2(\mathbb{H})$ on the upper half-plane $\mathbb{H}$. Practically, this means that $\hat{\psi}(\omega) = 0\ \forall \omega < 0$ (this is a direct consequence of Titchmarsh's theorem). Such a wavelet is necessarily complex; an example of such a function is the Morlet wavelet ψ_M whose Fourier transform is

$$\hat{\psi}_M(\omega) = \exp\left(-\frac{(\omega-\Omega)^2}{2}\right) - \exp\left(-\frac{\omega^2}{2}\right)\exp\left(-\frac{\Omega^2}{2}\right),$$

where Ω is called the central frequency. One generally chooses $\Omega = \pi\sqrt{2/\log 2}$ so that the ratio between the two largest maxima is $1/2$. This is obvious, since for such a value, the period of $\cos(\Omega x)$ is $\sqrt{\log 4}$ and $\psi_M(\sqrt{\log 4}) = 1/2$. A wavelet $\psi \in H^2(\mathbb{H})$ allows to recover a characteristic frequency through the modulus of the CWT. One directly gets

$$W[\cos(\omega_0 x)](t,a) = \frac{1}{2}\exp(i\omega_0 t)\hat{\bar{\psi}}(a\omega_0). \tag{1}$$

For the Morlet mother wavelet, the maximum of $\hat{\psi}_M(\cdot\,\omega_0)$ is reached for $a = \Omega/\omega_0$. If a_0 denotes this maximum, one gets $\omega_0 = \Omega/a_0$. The CWT can thus be used in a way similar to the windowed Fourier transform (here, the inverse of the scale plays the role of the frequency). The two main advantages of the CWT are the following:

- The scale a defines an adaptative window: the (numerical) support of $\psi(\cdot/a)$ is smaller for higher frequencies.
- One generally chooses a mother wavelet whose first m moments vanish, so that the associated CWT is orthogonal to lower degree polynomials, i.e. $W[f+P] = W[f]$, for any polynomial P of degree lower than m. In particular, trends do not affect the CWT.

3.3 The scale spectrum

Most of the Fourier spectrum-based tools are rather inefficient for non-stationary signals. The CWT provides a method that is relatively stable for signals whose properties do not evolve too quickly: the so-called scale spectrum (see e.g. [25,26,5,3]). The scale spectrum of a signal s is, following [26,27],

$$\Lambda(a) = E|W[s](t,a)|,$$

where E denotes the mean over time t. It can be shown that the scale spectrum is a rather efficient method to detect cycles in a signal, even if it is perturbed with a colored noise or if it involves "pseudo-frequencies" [26,27,5].

Let us emphasize, as did [25], that the scale spectrum has a very different meaning from the Fourier spectrum. When looking at a Fourier spectrum, the existence of energy at a given frequency means that a component of a sine (or cosine) wave persisted through the whole time span of the signal. The presence of energy at the same frequency in the scale spectrum only means that, in the whole time span of the signal, there is a higher likelihood for such a wave to have appeared locally. Unlike the Fourier transform, the scale spectrum can thus be used to study non-stationary signals.

Let us remark that the scale spectra computed in this work do not take into account values that are subject to border effects. This severely restrains the number of observable frequencies (the lowest frequencies are unreachable) but ensure that the scale spectrum is not subject to border artefact.

The accuracy of the cycles observed through the scale spectrum has been roughly estimated in [5], adding a Gaussian white noise to the signal. In any case, one can consider that the error is lower than 10%, which is sufficient to say that the cycles detected in this work (i.e. 30 and 43 months, see Section 4) are distinct.

3.4 Significance of the cycles

The significance of the observed cycles can be tested through a "red" noise model.

To check if the cycles appearing in the time series did not occur by pure chance, the spectra have been compared with a red noise random process, in which cycles could occur fortuitously. Such a red noise can be modeled by using an AR(1) model (autoregressive model of the first order):

$$x_n = \alpha x_{n-1} + \sigma\eta_n, \tag{2}$$

where η_n is a Gaussian white noise with zero mean and unit variance. Such processes are particularly important for their presence in many climatic and geophysical data (see e.g. [28, 29]). The first step consists in determining the two parameters in the process (namely α and σ) from the data. Once they are obtained, $N = 10,000$, say, realizations are generated and the scale spectrum of each so-obtained signal is computed. The last step consists in comparing the scale spectrum of the original data with the mean spectrum of the realizations. Following Chebyshev's inequality, the significance of a maximum in a can be checked by obtaining the greatest number k for which the relation

$$\Lambda(a) - (\bar{\Lambda}_N(a) + k\sigma_N(a)) > 0 \tag{3}$$

holds, where Λ is the scale spectrum of the data, $\bar{\Lambda}_N$ is the mean scale spectrum of the realizations and σ_N is the associated standard deviation.

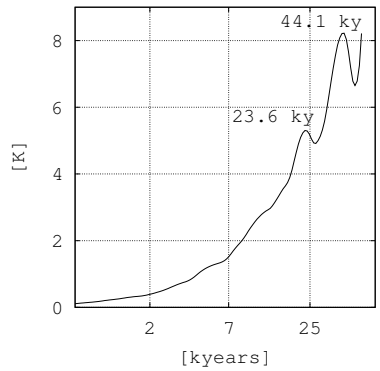

Fig. 1. Scale spectrum of the EPICA Dome C temperature data. The two maxima detected correspond two the precession and the obliquity.

4 Results

The methodology exposed in the previous section is applied here to different climatic datasets. First we show that it allows to recover well known astronomical cycles. Then, we apply this technique to millennial temperature reconstruction data to reveal the presence of two cycles of period 30 and 43 months. These cycles have been previously observed in weather station temperature data in [5] (for the period 1950–2007). We then focus on the possible relation between the main climatic indices and these cycles. The NCEP/NCAR data establish their presence on the whole planet. Finally, it is shown that they are significant.

4.1 EPICA Dome ice core deuterium data

The scale spectrum obtained from the EPICA deuterium data is shown at Figure 1. Two maxima are observed, corresponding to period cycles of 23.6 and 44.1 ky. These cycles agree with the Milanković theory concerning the precession and the axial tilt (obliquity) of the Earth [30,31], whose periods are known to be approximatively equal to 23 ky and 41 ky respectively. The scale spectrum shape clearly shows that the amplitude of the smallest period cycle detected (23.6 ky, corresponding to the precession) is smaller than the axial tilt cycle amplitude. In this context, the amplitude of the 23.6 ky cycle is about 5.5 K and the one associated to the 41.1 ky cycle is 8 K. Let us remark that the data length is not sufficient to allow the detection of the cycle related to the eccentricity (with a period approximatively equal to 100 ky). Moreover, no cycle about 19 ky has been observed in the EPICA data; indeed, the Fourier spectrum of the same records does not display such a cycle either, suggesting a low impact of this period on the EPICA Dome C data. Nonetheless, it is not clear that a lower amplitude 19 ky period can be distinctly separated from the 23 ky period (see [5]); it is thus possible that the cycle related to 19 ky exists but remains hidden by the one corresponding to 23 ky in the scale spectrum. To validate these results obtained with the wavelet tool, we have applied the same methodology to the parameters of the orbit of the Earth, obtained from the *orbit91* data file [30], retrieved at `ftp://ftp.ncdc.noaa.gov`. The cycle periods found are: 22.4 ky for the climatic precession, 40.4 ky for the axis obliquity and 99.4 ky for the eccentricity of the orbital movement around the Sun.

4.2 Hemispheric temperature reconstructions using palaeoclimatic records

The scale spectra obtained from the high-resolution palaeoclimatic records for the last millennium for both hemispheres [8], allows us to detect a 2.35 y (i.e. about 28.2 months) period

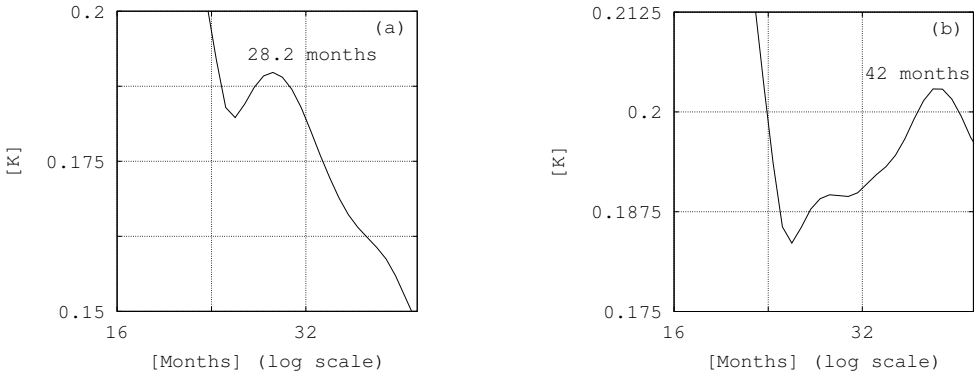

Fig. 2. Scale spectra of the Jones millennial temperature reconstructions data. (a) Northern Hemisphere, (b) Southern Hemisphere.

Table 1. Global temperature cycle periods detected in [5]

Data time series	Northern Hemisphere	Southern Hemisphere
CRUTEM3	2.5 ± 0.2 y	3.6 ± 0.2 y
GLBTs	3.5 ± 0.2 y	3.6 ± 0.2 y

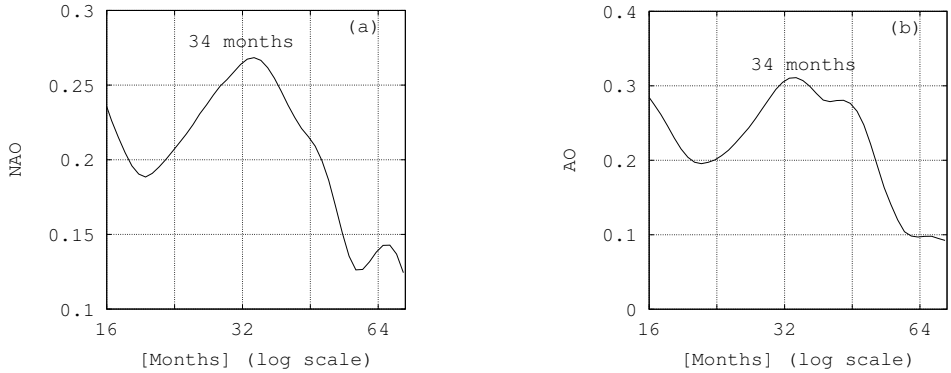

Fig. 3. Scale spectra of the (a) NAO CPC index and the (b) AO CPC index.

cycle for the Northern Hemisphere and a 3.5 y (i.e. 42 months) period cycle for the Southern Hemisphere (see Fig. 2). However, the small number of proxy indicators used to build these data does not allow us to assert that the observe cycles are hemisphere-dependent. The difference of period in the detected cycles could, for example, depend on the climate area. Moreover, the 28 months pseudo-period is also present on the Southern Hemisphere (see Fig. 2 (b)). However, these "minor" cycles cannot be resolved by the used method, as they are hidden by the major ones.

These cycles have already been found in [5] in global temperature time series from CRUTEM3 and GLBTs (see Table 1). Although the sources of the temperature reconstructions and the sampling period lengths are different, cycle amplitudes are quite similar (0.1 and 0.2 K). In [7], the analysis of the monthly air temperatures time series from the Prague-Klementinum weather station (1781-2002) has also lead to the detection of the same type of cycle with a period of 2.2 y. It is also shown in [6] that this cycle in temperature and the corresponding one in the NAO index are phase-coherent. Concerning the Jones data sets (NH10 and SH7), the existence of the periodicities observed on the scale spectra suggests the continuity of the cycles during a long part of the last millennium.

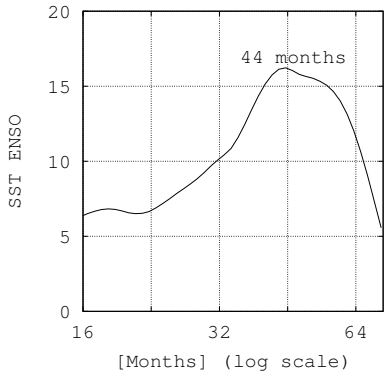

Fig. 4. Scale spectrum of the Global SST ENSO index.

Table 2. Cycles found in some world weather stations; the errors are estimated as in [5]. The stations were selected to represent the main climatic areas. For the class of climates, see [32].

Weather stations	Lat.	Long.	Cycle period	Cycle amp.	Annual amp.	Clim. classif.
Uccle (Belgium)	50.8°N	4.3°E	30.4 ± 2.7 m	0.4 K	15 K	DO
Zaragoza (Spain)	41.6°N	0.9°W	28.4 ± 2.4 m	0.3 K	18 K	BS
The Pas (Canada)	54.0°N	101.1°W	$28.5 \pm 2.6/44.8 \pm 2.4$ m	0.6/0.8 K	38 K	EC
Fairbanks (Alaska)	64.8°N	147.9°W	$28.5 \pm 2.5/40.4 \pm 2.5$ m	0.8/0.8 K	40 K	EC
Verhojansk (Siberia)	67.5°N	133.4°E	31.7 ± 2.5 m	0.8 K	64 K	EC
Jakutsk (Siberia)	62.0°N	129.7°E	28.6 ± 2.4 m	0.8K	60 K	EC
San Francisco (California)	37.6°N	122.4°W	41.8 ± 2.7 m	0.3 K	8 K	Cs
Lander (Wyoming)	42.8°N	108.7°W	41.8 ± 2.6 m	0.6 K	28 K	DC
Manaus (Brazil)	3.1°S	60.0°W	43.3 ± 2.4 m	0.3 K	3 K	Ar
Belo Horizonte (Brazil)	19.9°S	43.9°W	41.8 ± 2.4 m	0.5 K	4 K	Aw
Tahiti (French Polynesia)	17.6°S	149.6°W	41.8 ± 2.5 m	0.2 K	3 K	Ar
Lihue (Hawaii)	22.0°N	159.3°W	41.8 ± 2.5 m	0.3 K	4 K	Ar
Colombo (Sri Lanka)	6.9°N	79.9°E	44.5 ± 2.6 m	0.2 K	2 K	Ar
Minicoy (India)	8.3°N	73.2°E	41.8 ± 2.6 m	0.2 K	2 K	Aw

4.3 Air surface temperatures in the climatic regions under the influence of the AO, NAO and ENSO indices

Advection causes the transfer of air masses to neighboring regions and carries, throughout its trajectory, the atmospheric properties including air temperature. Climatic indices characterize and synthesize these air mass movements. The data series used in this paragraph are also truncated before 1950 to permit the comparison between the different results. This length only allows to find cycles with period lower than 5 y. The shape of the NAO CPC scale spectrum exhibits a maximum corresponding to a 34 months cycle period. A second maximum, which concerns a 68 months (5.7 y) period, is also detected. Concerning the AO CPC monthly scale spectrum, the region corresponding to abscissa in between 30 months and 50 months features two maxima, corresponding to two cycles; the first one, which describes a 34 months period, corresponds to the cycle detected in the NAO CPC data time series, and the second one, smaller than the first, identifies a 43.3 months period. This non-trivial result probably underlines that the global impacts of ENSO can even be detected in the Arctic region, supporting results of e.g. [33]. The scale spectrum computed from the Global SST ENSO data series, allows us to detect a 44.8 months period. Temperature time series from more than one hundred weather stations have been processed and the results (see [5]) show a strong relation between the weather stations localization and the influence areas of the relevant climatic indices. Table 2 shows some of these weather stations (as well as their locations, the cycle periods observed, the amplitudes

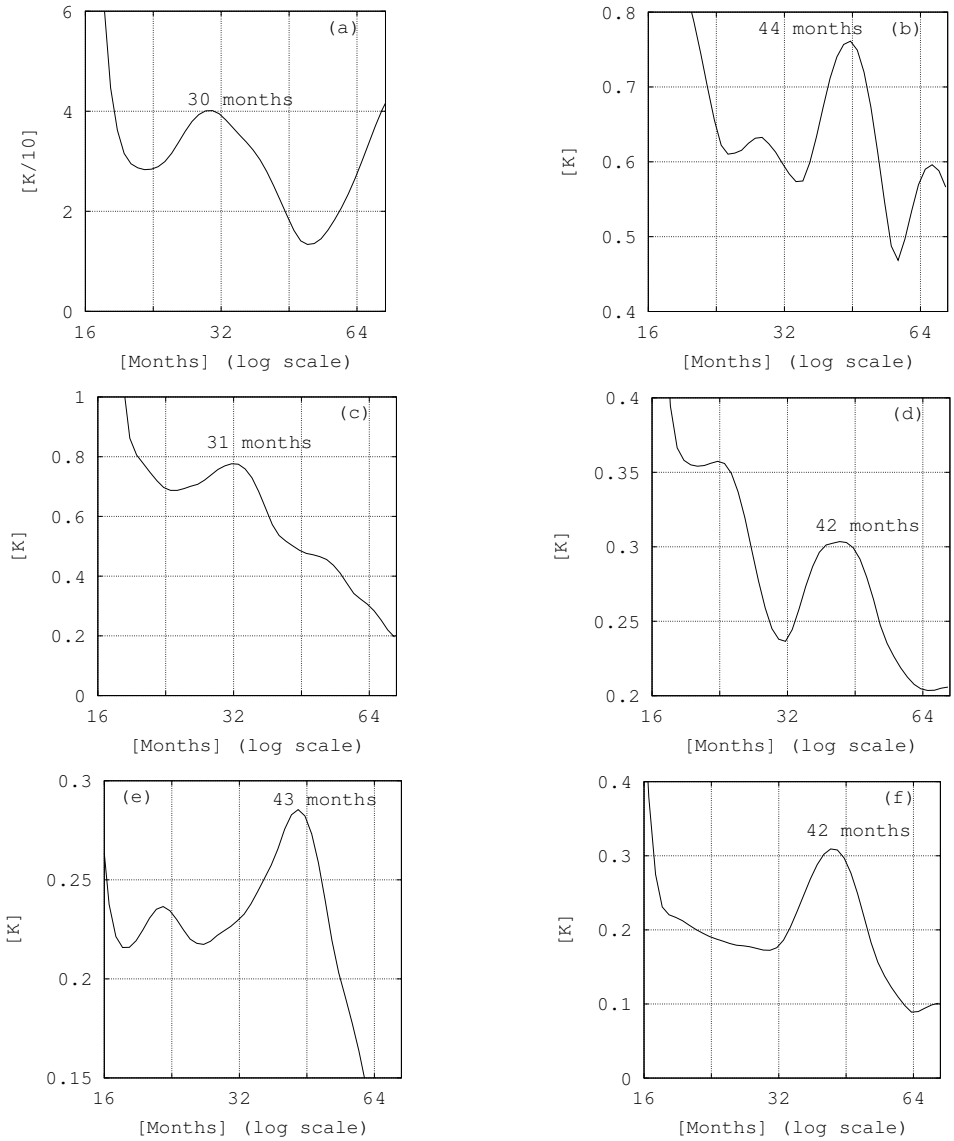

Fig. 5. Scale spectra of some air temperature data. (a) Uccle (Belgium), (b) The Pas (Canada), (c) Verhojansk (Siberia), (d) San Francisco (California, USA), (e) Manaus (Brazil), (f) Lihue (Hawaii, USA).

measured and the associated class of climate); they were selected to cover most of the typical climate areas (see [32] for more details). Let us also remark that the scale spectrum leads to a correct estimation of the annual temperature amplitude, i.e. the difference between the mean temperatures of the warmest and the coldest months (see Table 2). The European, North-American and some Siberian weather stations are subject to cycles (30 months period) that also occur in the air mass advections characterized by the AO and NAO indices (34 months period). Air temperatures for other areas, like California, Brazil, Caribbean Sea and Hawaii, are dominated by cycles similar to those found in the Global-SST ENSO (44.8 months). The North-American weather station time series analysis shows the presence of the two cycles that tends to suppose the influence of ENSO over areas already affected by the Arctic and North-Atlantic oscillation.

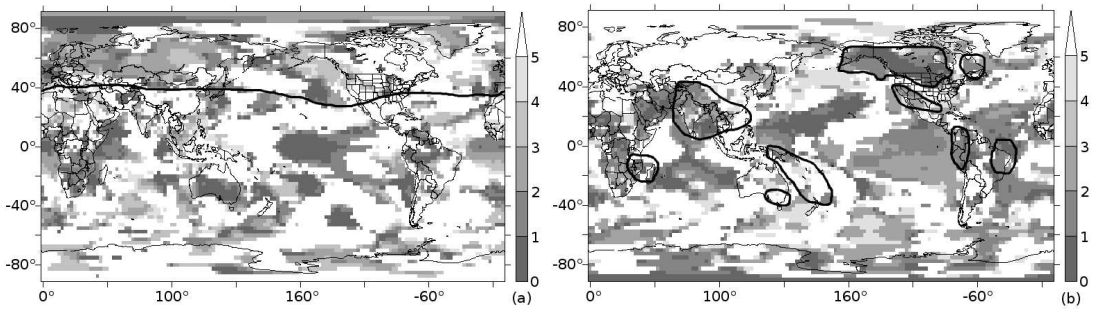

Fig. 6. NCEP/NCAR reanalysis data. The regions of the globe where a cycle corresponding to either 30 (left panel) or 42 months (right panel) has been detected on the grid points are colored using a color palette going from gray (corresponding to the period of 30 months in the left panel and 42 months in the right panel) to white (if no cycle is detected within a tolerance of ± 5 months). The zone of influence of the AO index can be roughly defined as the region above the thick line in the left panel. The zones of influence of the ENSO index (concerning the temperatures) are circled with thick lines in the right panel.

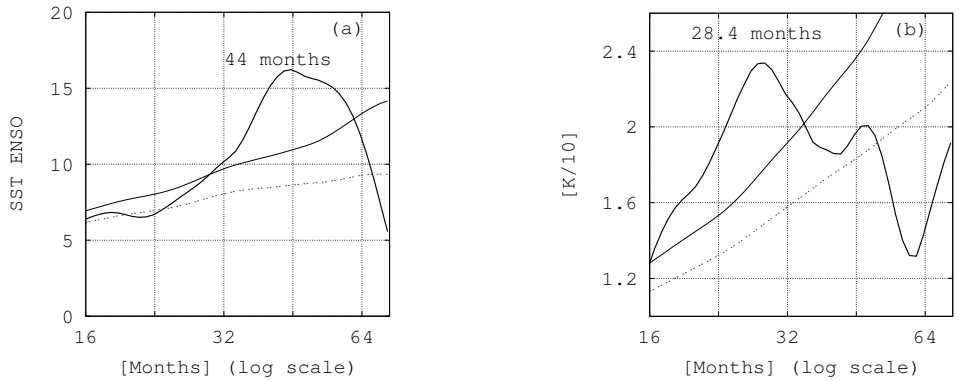

Fig. 7. The detected cycles are significant, following the method described in subsection 3.4. (a) The scale spectrum Λ of the ENSO index (thick line) vs. the mean scale spectrum $\bar{\Lambda}$ of the associated red noise (dashed gray thin lines) and $\bar{\Lambda} + \sigma$ (black thin line). (b) The air temperature data from Zaragoza are used instead of ENSO.

In order to show that the above cycles cover the whole planet, the NCEP/NCAR time series were analyzed using the scale spectrum method. As shown in Fig. 6, most of the grid points do present a cycle corresponding to either 30 or 42 months. Indeed, when projecting the grid points onto the planisphere, 92.7% of the so weighted pixels display such a cycle. Moreover, the regions displaying one of the cycles are in relative good agreement with the influence zones of the AO, ENSO and NAO indices (see Fig. 6).

4.4 Significance of the observed cycles

The crucial question raised by these observations is to know whether or not the detected cycles can be considered as significant. This is indeed the case.

The method described in subsection 3.4 has been applied to the Jones millennial temperature reconstructions time series (NH10 and SH7), the CRUTEM3 air temperature data, the chosen climatic indices (AO,NAO and ENSO) and to the selected weather station air temperature data. For each of these signals, $N = 10,000$ realizations of the process defined by the relation (2) have been generated and the greatest number k such that inequality (3) holds, with a corresponding to 30 or 42 months, has been computed. These numbers k are reported in Table 3 .

Table 3. Values of the greatest number k satisfying inequation (3) for the scales corresponding to 30 or 42 months.

Data time series	cycle	k
ENSO	43	3.4
AO	32	6.6
NAO	33	4.7
NH10	28	3.3
SH7	43	1.3
Uccle	30.4	3.9
Zaragoza	28.4	3.14
The Pas	28.5/44.8	3.1/3.2
Fairbanks	28.5/40.4	3.5/3.5
Verhojansk	31.7	4.7
Jakutsk	28.6	7
San Francisco	41.8	4.2
Lander	41.8	4
Manaus	43.3	8.2
Belo Horizonte	41.8	8.2
Tahiti	41.8	8.6
Lihue	41.8	9.6
Colombo	44.5	8.4
Minicoy	41.8	3.6

5 Concluding remarks

The wavelet methodology presented in Section 3 has been applied to palaeoclimatic data, air temperature and reanalysis time series as well as data related to climatic indices.

The scale spectrum associated to the EPICA DOME C ice core deuterium data displays two maxima corresponding to the precession and the obliquity of the Earth periods. The third Milanković cycle (whose associated period is about 100 ky) is out of range of our approach, because of the length of the data at our disposal.

The cycles of 30 and 43 months previously detected in [5] are also observed in the proxy data of Jones millennial temperature reconstruction. This is indeed an argument in favor of the persistence of these cycles through time. The scale spectra related to the NCEP/NCAR time series show that 92.7% of the grid points display at least one of the above-mentioned cycle. The same rhythm is usually observed in a climatic index and in the regions under its influence, although no significant correlation can be obtained with this method. These results are corroborated by the temperature time series of individual weather stations obtained from the ECAD and GISS data sets (only the most complete signals were kept). The variation of the temperature amplitude induced by these cycles is always between 0.2 and 0.8 K. This amplitude is about ten percents of the annual amplitude. It is also shown, comparing the data to a red-noise model, that the observed cycles are significant.

The wavelet spectrum is a particularly well shaped tool for the study of temperature data, since it allows to detect cycles in non-stationary signals. However, further work has to be done in order to obtain more accurate error bounds. This would also be useful to prove that the two observed cycles are clearly distinct. This will be the subject of a forthcoming paper.

Acknowledgments

The authors would like to express their gratitude to the members of the Center for Is og Klima in Copenhagen; in particular, we thank P. Ditlevsen for providing fruitful discussions. We also have to thank X. Fettweis (from the University of Liège) for his comments.

References

1. D. Gu, S.G.H. Philander, J. Climate, **8**, (1995) 864
2. B. Wang, Y. Wang, J. Climate, **9**, (1996) 1586
3. C. Torrence, G.P. Compo, Bull. Amer. Meteorol. Soc., **79** (1998), 61
4. S. Jevrejeva, J.C. Moore, P.L. Woodworth, A. Grinsted, Tellus A, **57**, 183
5. S. Nicolay, G. Mabille, X. Fettweis and M. Erpicum, Climate Dynamics, (2009) to appear
6. M. Palus, D. Novotna, Nonlinear Proc. Geophys., **13**, (2006) 287
7. M. Palus, D. Novotna, *Detecting oscillations hidden in noise: Common cycles in atmospheric, geomagnetic and solar data.* In: R. Donner, S. Barbosa (eds), Nonlinear Time Series Analysis in the Geosciences, Springer, Berlin, (2008) 327
8. P.D. Jones, K.R. Briffa, T.P. Barnett, S.F.B. Tett, The Holocene, **8**, (1998) 455
9. EPICA community members, Nature, **429**, (2004) 623
10. J. Jouzel et al, Science, **317**, (2007) 793
11. A.M.G. Klein Tank et al, Int. J. Climatol., **22**, (2002) 1441
12. J. Hansen, R. Ruedy, J. Glascoe, M. Sato, J. Geophys. Res., **104**, (1999) 30997
13. E. Kalney et al., Bull. Amer. Meteorol. Soc., **77**, (1996) 437
14. A. Barnston, R. Livezey, Mon. Weather Rev., **115**, (1987) 1083
15. S. Zhou, A.J. Miller, J. Wang, J.K. Angell, Geophys. Res. Lett., **28**, (2001) 4107
16. I. Daubechies, *Ten lectures on wavelets*, SIAM, Philadelphia (1992)
17. S. Mallat, *A wavelet tour of signal processing*, Academic Press, New-York (1999)
18. Y. Meyer, *Ondelettes et opérateurs*, Hermann, Paris (1989)
19. P. Goupillaud, A. Grossman, J. Morlet, Geoexploration, **23**, (1984) 85
20. R. Kronland-Martinet, J. Morlet, A. Grossmann, International J. of Pattern Recogn. and Artificial Intellig., **1**, (1987) 273
21. A. Arneodo, G. Grasseau, M. Holschneider, Phys. Rev. Lett., **61**, (1988) 2281
22. A. Arneodo, Y. d'Aubenton Carafa, E. Bacry, P. Graves, J.-F. Muzy, C. Thermes, Physica D, **96**, (1996) 291
23. A. Arneodo, B. Audit, N. Decoster, J.-F. Muzy, C. Vaillant, *Climate disruptions, market crashes and heart attacks*. In: A. Bunde, H. Schellnhuber (eds), *The science of disasters*, Springer, Berlin, (2002) 27
24. S. Jaffard, S. Nicolay, Appl. Comput. Harmon. Anal., **26**, (2009) 181
25. N.E. Huang, S.R. Long, Z. Shen, Adv. Appl. Mech., **32**, (1996) 59
26. S. Nicolay, F. Argoul, M. Touchon, Y. d'Aubenton-Carafa, C. Thermes, A. Arneodo, Phys. Rev. Lett., **93**, 108
27. S. Nicolay,*Analyse de séquences ADN par la transformée en ondelettes*, Thèse de l'Universite de Liège (2006)
28. M.R. Allen, A.W. Robertson, Climate Dynamics, **12** (1996) 775
29. D.B. Percival, A.T. Walden, *Spectral Analysis for Physical Applications*, Cambridge University Press, Cambridge (1993)
30. A. Berger, M.F. Loutre, Quaternary Sciences Review, **10**, (1991) 297
31. M. Milanković, *Kanon der Erdbestrahlung und seine Anwendung auf das Eiszeitenproblem*, R. Serb. Acad., Belgrade (1941)
32. W. Rudloff, *World–Climates*, Wissenschaftliche Verlagsgesellschaft mbH, Stuttgart (1981)
33. S. Jevrejeva, J.C. Moore and A. Grinsted, Geophys. Res. Lett., **31**, (2004) L24210